Materials Science & Engineering A 606 (2014) 322–329

Contents lists available at ScienceDirect

Materials Science & Engineering A

journal homepage: www.elsevier.com/locate/msea

Enhanced mechanical properties in friction stir welded low alloy steel joints via structure refining

P. Xue *, Y. Komizo, R. Ueji, H. Fujii

Joining and Welding Research Institute, Osaka University, 11-1 Mihogaoka, Ibaraki, Osaka 567 0047, Japan

ARTICLE INFO

Article history:
Received 6 January 2014
Received in revised form
26 February 2014
Accepted 17 March 2014
Available online 24 March 2014

Keywords:
Friction stir welding
Bainite
Grain refinement
Microanalysis
Mechanical characterization

ABSTRACT

Submerged arc weld metal of a high strength low alloy steel was subjected to friction stir welding (FSW) at a higher rotation rate of 400 rpm (FSW-a) and a lower rotation rate of 125 rpm (FSW-b), respectively. The microstructures and mechanical properties of three typical phase structures, coarse bainite phase in the weld metal, refined bainite phase and ferrite phase in the nugget zones (NZs) of FSW joints were investigated. Compared to the weld metal, enhanced mechanical properties were achieved in the NZs of both FSW joints. Large cracks apparently propagated along the bainite lath in the coarse grains of the weld metal, which would cause the brittle quasi-cleavage fracture. However, large crack propagation was inhibited in the refined bainite phase structure in the NZ of FSW-a joint, and enhanced strength and toughness with dimple fracture were achieved. Meanwhile, enhanced mechanical properties, including strength and ductility, as well as toughness, were obtained in the NZ of FSW-b joint, because of the refinement of the ductile ferrite structure.

1. Introduction

In recent years, high strength low alloy (HSLA) steels have attracted considerable interest in various industrial areas, such as oil and gas transportation, ship building, and automotive industries [1–3]. In the fabrication of HSLA steel structures, the integrity and reliability of structures are extremely dependent on the mechanical properties of the welded joints. However, the growth of prior austenite grains during fusion welding process will lead to poor mechanical properties, especially when the formation of coarse bainite and martensite phases occurs. Therefore, the control of the microstructure in the welded joints for obtaining sound strength-toughness synergy should be the key issue for the actual application of HSLA steels [4,5].

It is well accepted that grain refining is an essential strengthening method that enhances both the strength and the toughness of the metal materials simultaneously. Therefore, various grain refining methods have been used for refining the weld structure of HSLA steel joints. Inclusion assisted microstructure control is the most encouraging method to refine the weld metal, with the formation of fine intragranular acicular ferrite (AF) [5–8]. Though a fine interlocking AF structure with the average grain size of less than 5 μm can be produced, some coarse grains larger than 10 μm usually form in the weld metal, especially at the prior austenite grain boundaries [5,9,10]. Besides, in order to increase the strength without significant loss in toughness, bainite phase structure is desirable in the weld metal. However, very large bainite laths usually form in the coarse prior austenite grains, which may result in the easy propagation of large cracks along the lath boundaries [11,12]. In this case, other methods are still needed for obtaining a uniform refined microstructure in the HSLA steel joints.

Friction stir welding (FSW) is a solid state technology which could eliminate the melting and solidification associated problems, such as liquation and solidification cracking [13,14]. Since invented in 1991, FSW has been successfully applied to various types of materials, such as Al, Mg, Cu alloys [13–17]. Recently, FSW of high melting point alloys including Ti, Ni-based alloys, and also steels, has been increasingly drawing attention [18–24]. Though FSW is characterized as a solid-state process, the peak temperature is usually higher than A_{C1}, i.e. the α–γ phase transformation temperature, in FSW of steel [19]. Therefore, transformed phase structures, martensite and bainite phases usually appear in the nugget zone (NZ). However, due to the intense plastic deformation, the prior austenite grain size should be greatly refined compared to that in the conventional fusion welding [19–24]. Then, the mechanical properties may be enhanced in the NZ of FSW joint, especially when the bainite forms.

On the other hand, the heat input could be reduced greatly if a very low rotation rate is adopted during FSW, and the peak temperature could be controlled to below A_{C1} [25,26], bring about the fine ductile ferrite structure. Therefore, if we control the rotation rates, different peak temperatures of above and below

* Corresponding author.
E-mail address: pxue@imr.ac.cn (P. Xue).

http://dx.doi.org/10.1016/j.msea.2014.03.058
0921-5093/

A_{C1} can be achieved during FSW. Then, various refined microstructures with/without phase transformations will be obtained in the NZs, and this will inevitably bring different mechanical properties. It is interesting to compare the mechanical performances of these special microstructures with the weld metal in fusion joints; however, related investigations are still lacking.

In this study, a submerged arc weld metal was subjected to FSW at a higher rotation rate of 400 rpm and a lower rotation rate of 125 rpm, resulting in different peak temperatures of above A_{C3} and below A_{C1} in the NZs, respectively. In this case, three different typical phase structures, coarse bainite phase in the weld metal of fusion joint, fine bainite phase and ferrite phase in the NZs of FSW joints were achieved. The investigations of the microstructure evolution and mechanical properties in the NZs of the FSW joints, as well as the relationship between the microstructure and mechanical behaviors of the three typical phase structures were carried out in this study.

2. Experimental procedures

The materials used in this study were HSLA steel weld plates fabricated by submerged arc welding (SAW), and the chemical composition of the weld metal is shown in Table 1. In order to investigate the intrinsic differences of the mechanical properties between the fusion weld metal and the NZs of FSW joints, FSW was performed on the SAW weld metal, and thus the chemical compositions should be the same. After SAW, the weld plates were machined to 300 mm length, 100 mm width and 2 mm thickness blocks. FSW experiments were performed using a load-controlled FSW machine, and an argon (Ar) shielding gas was used to prevent the oxidation of the weld surface during FSW. Two FSW parameters of 400 rpm–200 mm/min and 125 rpm–100 mm/min were used in this study, designated as FSW-a and FSW-b, respectively. The welding tool was made of a tungsten carbide (WC) based material and equipped with a columnar pin without threads. The tool size and FSW parameters are shown in Table 2.

Microstructural observations were conducted by optical microscopy (OM), electron backscatter diffraction (EBSD), and scanning electron microscopy (SEM). The specimens for OM and SEM observation were machined perpendicular to the welding direction, and etched with a 4% nital solution. EBSD specimens were prepared by electro-polishing at room temperature using a solution of 92% acetic acid and 8% perchloric acid under a potential of 30 V.

Vickers hardness tests of the FSW joints were measured on the cross-section perpendicular to the welding direction at the center of the NZ. For each measurement, 1000 g load was applied for 15 s at intervals of 0.5 mm. The dog-bone-shaped tensile specimens with a gauge of 3 mm length, 1.4 mm width and 0.7 mm thickness were machined perpendicular to the welding direction from the weld metal and NZs, as schematically shown in Fig. 1. Uniaxial tensile tests were conducted at an initial strain rate of $1 \times 10^{-3}\ s^{-1}$. The fracture surfaces were examined using SEM.

Mini-specimens for Charpy impact tests were cut from the weld metal and NZs in a direction perpendicular to the welding direction to dimensions of 20 mm length, 0.5 mm thickness, and 0.5 mm width, and all samples were given a 0.1 mm notch (Fig. 1). A miniaturized Charpy impact machine, developed earlier [27], was employed to determine energy absorption under dynamic fracture. The samples were impacted with a punch driven by a pressurized gas cylinder, with impact load measured by a load cell placed at the top of the punch. Impact testing was carried out at the room temperature, with the impact deformation rate (i.e. the speed of the punch) of $1\ ms^{-1}$.

3. Results

Fig. 2 shows the macrostructures of the SAW weld metal and FSW joints. The weld metal exhibited a typical fusion welded structure, with many coarse columnar grains, as shown in Fig. 2a. Defect-free NZs were successfully achieved by both FSW parameters, and the microstructures were refined apparently (Fig. 2b and c). The macrostructure of the FSW joint revealed a "bowl" shape, indicating an intense plastic deformation occurrence during FSW owing to both shoulder and pin effect.

Fig. 3 shows the detailed microstructure of the weld metal. The weld metal was characterized as a typical bainite structure, with many large bainite laths in the coarse grains. Moreover, coarse grain boundary ferrite (GBF) phase formed at the prior austenite grain boundaries during the phase transformation of the welding process (Fig. 3a). From the SEM microstructure shown in Fig. 3b, many carbide strips between the bainite laths could be observed.

After FSW, the microstructure was greatly refined, and equiaxed grains were achieved in the NZs, as shown in Fig. 4. Bainite phase structure was obtained at a high rotation rate of 400 rpm (FSW-a). Compared to the weld metal, the bainite grain size was significantly decreased, and the largest grain size was about 10 μm. The distributions of various paralleled bainite laths in the fine equiaxed grains, and carbides between the bainite laths were confirmed (Fig. 4a and b). However, uniform equiaxed ferrite grains formed at a lower rotation rate of 125 rpm (FSW-b), indicating a peak temperature of below A_{C1} during FSW process. It is obvious that the grains in the NZ were further refined compared to that in FSW-a joint, with an average grain size of ~3 μm. Moreover, many ultrafined carbide precipitations distributed in the fine ferrite grains or the grain boundaries (Fig. 4d).

Table 1
Chemical composition of the weld metal (in wt%).

Element	C	Si	Mn	P	S	Cu	Ni	Cr	Ti	V	Nb	B	Al	O	N
Content	0.057	0.30	1.51	0.010	0.005	0.18	0.11	0.12	0.017	0.03	0.023	0.0030	0.034	0.027	0.0045

Table 2
Summaries of the welding conditions.

No.	Welding parameters			Tool size		
	Rotation rate (rpm)	Welding speed (mm/min)	Tool tilt	Shoulder diameter (mm)	Pin diameter (mm)	Pin length (mm)
a	400	200	3	12	4	1.8
b	125	100	3			

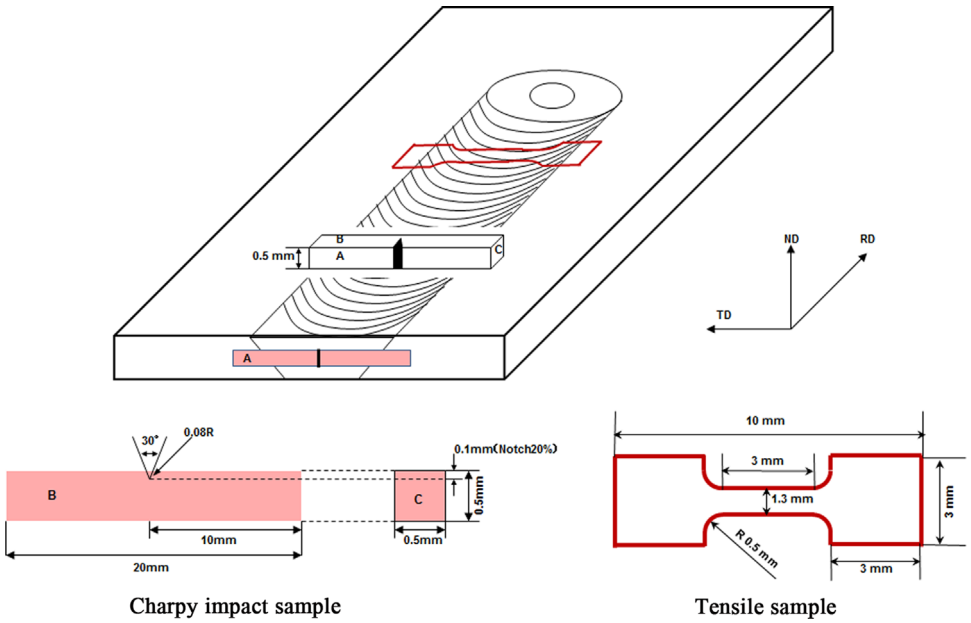

Fig. 1. Schematic illustration of the tensile and Charpy impact specimens.

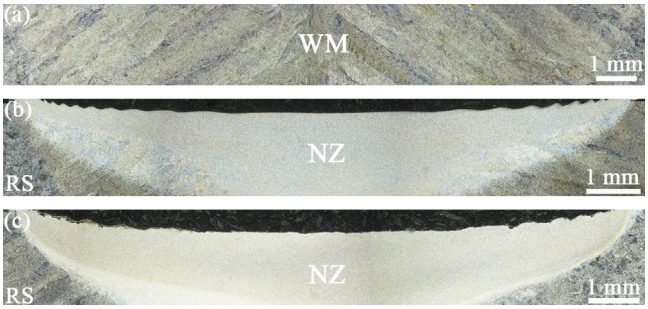

Fig. 2. Macrostructure of (a) weld metal (WM) and FSW joints with parameters of (b) 400 rpm–200 mm/min (FSW-a) and (c) 125 rpm–100 mm/min (FSW-b).

Fig. 5 shows the analysis results of the microstructures of the weld metal and NZs by EBSD. Coarse bainite grains were observed in the weld metal, and many low angle grain boundaries (LAGBs, misorientation angle $<15^{\circ}$) distributed in the coarse grains (Fig. 5a), which coincided well with the OM and the SEM results. Most of the LAGBs should be the bainite lath boundaries according to the previous studies [10,11,24]. However, many high angle grain boundaries (HAGBs, misorientation angle $\geq 15^{\circ}$) were characterized for the fine bainite structure in the NZ of the FSW-a joint. Similar to the weld metal, some LAGBs were also observed in the bainite grains, as shown in Fig. 5b. Differently, fine equiaxed ferrite grains in the NZ of FSW-b joint were characterized as predominantly HAGBs, while few LAGBs were observed (Fig. 5c).

Moreover, many retained austenite phases were observed in the weld metal (Fig. 5d), indicating that insufficient phase transformation occurred during the fusion welding process. However, very few retained austenite phase was observed in the NZs of FSW joints, as shown in Fig. 5e and f. Therefore, a more sufficient phase transformation could be speculated during FSW process due to the intense plastic deformation.

The distributions of grain size and misorientation angle for the weld metal and NZs are shown in Fig. 6. The average grain sizes were about 41.9, 3.9 and 2.8 μm for the weld metal and NZs of FSW-a and FSW-b joints, respectively, calculated automatically by the grain area determination method of the EBSD analysis software. As shown in Fig. 6d, the misorientation angle, because of the bainite phase transformation, concentrated at the LAGB area and 50–60° range compared to the random distribution of the cubic metals. The fractions of these two concentrated misorientation angles reduced in the NZ of FSW-a joint, and the fraction of HAGBs increased from 81.4% (the weld metal) to 91.7% (Fig. 6e). Similar distribution to the random distribution of the cubic metals was achieved in the NZ of FSW-b joint because of the absence of the phase transformation, and the fraction of HAGBs was as high as 95.4% (Fig. 6f).

From the hardness distribution of the FSW joints shown in Fig. 7, it is clear that relatively uniform hardness values were achieved in the NZs of both FSW joints. The average hardness value was 240 Hv for the weld metal, while increased to 340 Hv in the NZ of FSW-a joint. Moreover, slightly increased hardness value of 250 Hv was achieved in the NZ of FSW-b joint.

Fig. 8a shows the typical tensile curves of the weld metal and NZs in both FSW joints, and the tensile properties were summarized in Table 3. For the weld metal, the yield strength (YS) and the ultimate tensile strength (UTS) were 659 and 761 MPa, and the uniform elongation (UE) and fracture elongation (EL) were 6.3% and 23.0%, respectively. By refining the bainite grain size, greatly enhanced YS and UTS of 955 and 1056 MPa were achieved in the NZ of FSW-a joint, and the UE and EL slightly reduced to 4.6% and 19.5%, respectively. Though the YS slightly reduced to 634 MPa, the UTS increased to 850 MPa in the NZ of FSW-b joint. Moreover, the UE significantly increased to 11.6%, about twice of that in the weld metal, and the EL increased to 28.7%.

Fig. 8b shows the results of Charpy impact tests for the weld metal and NZs in both FSW joints. In this graph, force is plotted as a function of punch travel, with an intergration of the resulting curve denoting the absorbed energy of the fracture, as shown in Table 3. The absorbed energies of the weld metal and the NZs in FSW-a and FSW-b joints were about 190, 206 and 251 N mm, respectively.

SEM microstructure of the fractured surfaces for both tensile and impact tests of the weld metal and NZs are shown in Fig. 9. Obvious dimples were observed on all the fractured surfaces of the tensile samples (Fig. 9a–c). No brittle cleavage fracture was observed from the fractured surface in the NZ of FSW-a joint in spite of a very high UTS of 1056 MPa, indicating a good toughness. However, the quasi-cleavage fracture morphology was observed on the impact fractured surface of the weld metal (Fig. 9d), while the dimple fracture morphologies appeared on the fractured surfaces of the NZs for both FSW joints (Fig. 9e and f).

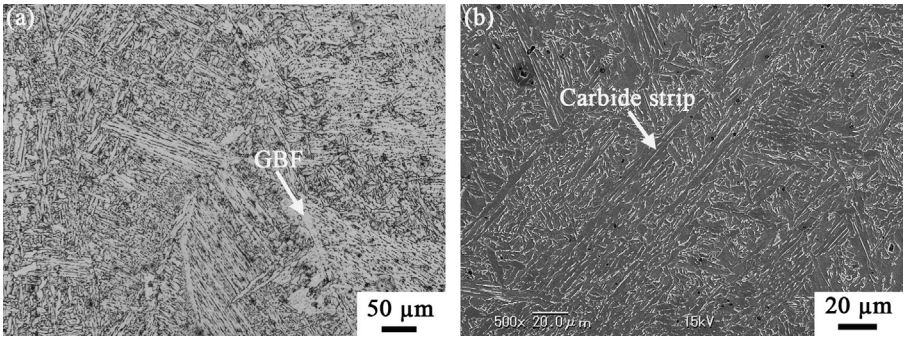

Fig. 3. Microstructure of the weld metal: (a) OM and (b) SEM.

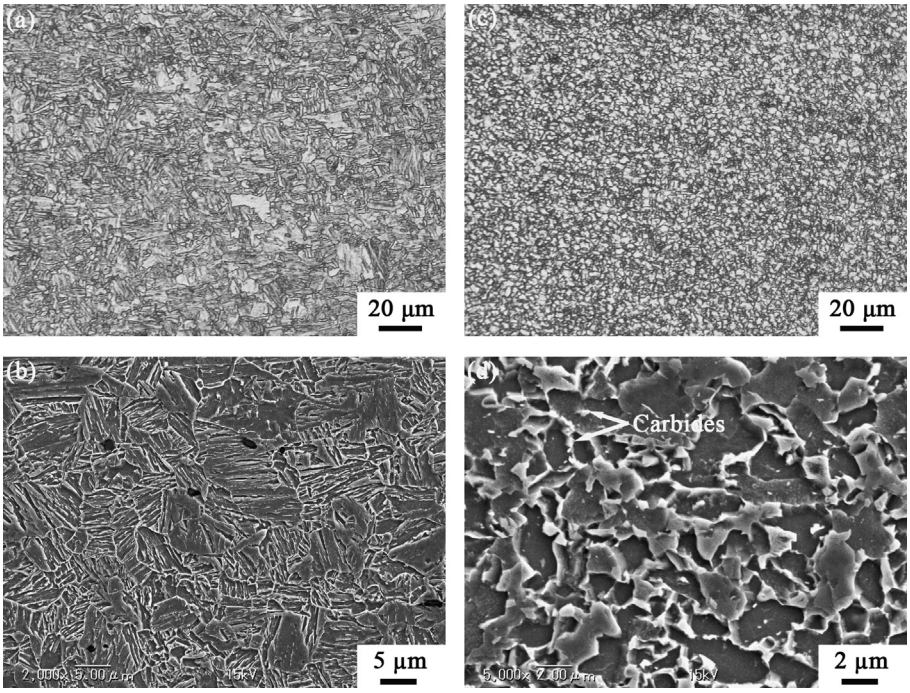

Fig. 4. Microstructure of the NZs in FSW-a joint: (a) OM, (b) SEM, and FSW-b joint: (c) OM, (d) SEM.

4. Discussion

An obvious refinement of the microstructures in the NZs of both FSW joints was obtained compared to that in the weld metal, which should be attributed to the dynamic recrystallization (DRX) process during FSW. In the NZ, the intense plastic deformation and thermal exposure resulted in the occurrence of DRX, thereby producing the remarkable microstructural refinement [13,14]. Usually, the heat input (thermal cycle) was closely related to the peak temperature and the heating time, which were mainly determined by the rotation rate and the traverse speed, respectively [28–30]. According to Sato et al. [30], the recrystallized grain size in the NZ increases exponentially with the peak temperature and linearly with the heating time, showing that the peak temperature exerts the dominant influence.

For the FSW-a joint, a relatively high rotation rate of 400 rpm was performed, indicating a higher peak temperature than A_{C3} according to previous studies [19,31]. This result could also be estimated from the transformed phase structure in the NZ, in which a main bainite phase structure was achieved with no ferrite phase formation (Fig. 4). Therefore, the metal should be heated into the austenite phase field (above A_{C3}) and plastically deformed around the FSW tool before experiencing cooling. In this case, the prior austenite grains were greatly refined by DRX under the intense plastic deformation. Then, the temperature began to reduce once the FSW tool had passed the NZ, and the austenite phase transformed to bainite phase during this cooling process, resulting in the fine bainite structure in the NZ as shown in Figs. 4 and 5. In this study, a high welding speed of 200 mm/min was chosen for FSW-a joint, bringing about a relatively high cooling rate. Previous studies indicate that the increase of the cooling rate will result in a higher likelihood of displacive transformation products (i.e., martensite and bainite) in the NZ [19,31,32]. Therefore, bainite phase was the main transformation product, and no ferrite phase formed in the NZ of the FSW-a joint.

On the other hand, it may be relatively simple for the grain refining process if the metal deforms below A_{C1}, like the FSW-b joint in this study [25,26]. Due to the very low rotation rate of 125 rpm, only DRX without phase transformation should occur at a low temperature (below A_{C1}) in the NZ. In this case, the ferrite phase will be refined by the DRX process from the initial bainite laths (actually the ferrite phase) during FSW. Moreover, the initial carbide strips will be broken under the intense plastic deformation, resulting in the formation of the ultrafined carbide precipitations, as shown in Fig. 4c. It is well accepted that the broken carbide precipitations together with the inclusions in the initial weld metal will provide abundant

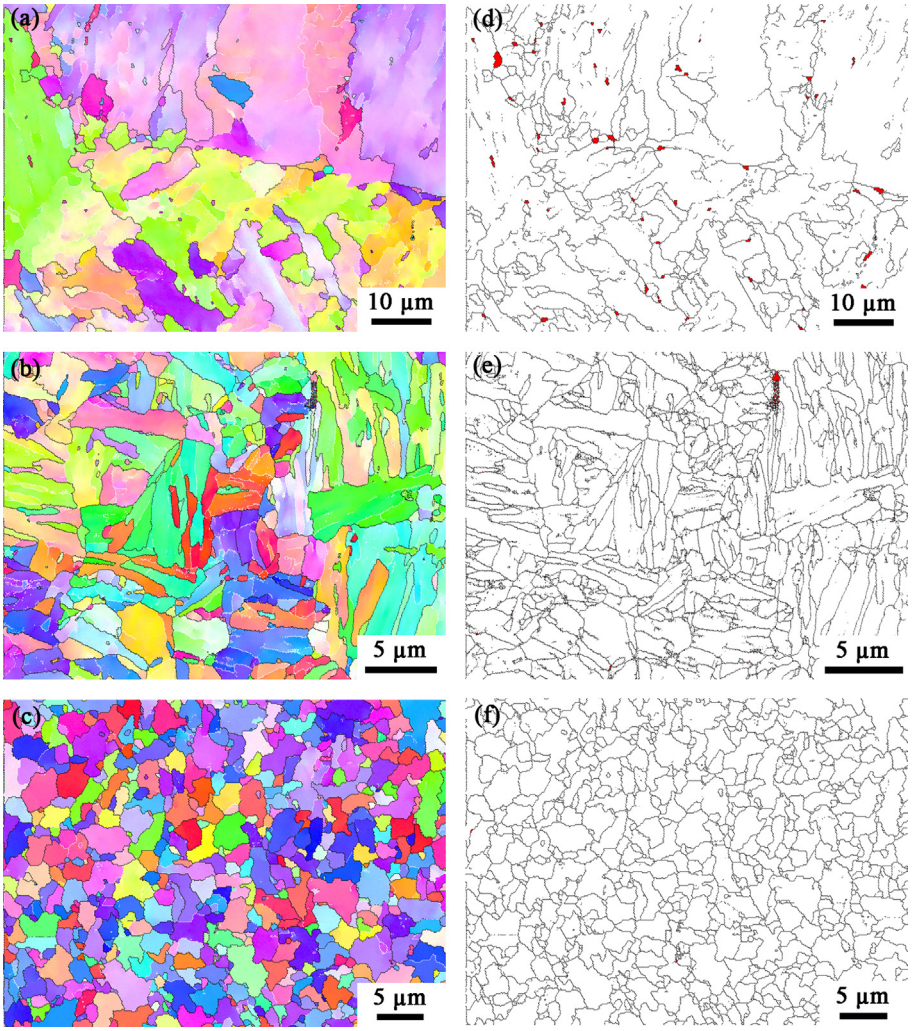

Fig. 5. EBSD microstructure of (a) weld metal, (b) NZ in FSW-a joint, (c) NZ in FSW-b joint (LAGBs and HAGBs are shown by white and black lines, respectively), and phase distribution maps of (d) weld metal, (e) NZ in FSW-a joint, (f) NZ in FSW-b joint (ferrite and austenite phases are shown by white and red, respectively). (For interpretation of references to color in this figure legend, the reader is referred to the web version of this article.)

recrystallization nucleus during DRX process, and thus very fine ferrite grains with an average grain size of 2.8 μm was achieved in the NZ of FSW-b joint.

It is well known that the mechanical properties of the welds in HSLA steels are primarily determined by the phase types and grain sizes [4,5,11]. The hardness and UTS were relatively high in the weld metal, 245 Hv and 761 MPa respectively, because of the formation of bainite phase structure, while further enhanced in the NZ of FSW-a joint, 350 Hv and 1056 MPa respectively, by the obvious refinement of the bainite grains. Though relatively soft ferrite phase formed in the NZ of FSW-b joint, the hardness and UTS still increased to 250 Hv and 850 MPa, respectively. This is because the ferrite grains were greatly refined, which had compensated the softening effect of the ferrite phase.

For the ductile ferrite phase, brittle cleavage seldom occurs during the mechanical tests, and the crack inhibition ability usually increases by reducing the grain size [25,26]. Therefore, in this study, the NZ of FSW-b joint exhibited sound tensile ductility and impact toughness, as shown in Figs. 8–10 and Table 3. However, when the bainite or the martensite phase forms in the welds, the bainite/martensite lath and packet size, and the prior austenite grain size, should be the primary factors affecting the post-weld properties [4,5,11]. Bainite packets are composed of bainite laths with LAGBs with a common crystallographic orientation [12]. In Fig. 3, very large prior austenite grain size and coarse bainite formed because of a very high peak temperature associated with higher heat input was achieved in the fusion welding process. Large cracks could be estimated to easily propagate along the bainite lath boundaries with LAGBs in the coarse bainite grains. Corresponding with this estimation, relatively straight large cracks could be observed in the weld metal from the SEM surface morphology after the impact test (Fig. 10a), and large cracks indeed propagated along the bainite lath boundaries (Fig. 10b).

Previous studies indicate that cleavage fracture resistance of bainite microstructure is closely related to both prior austenite grains and bainite packets since only high-angle bainite packet boundaries could efficiently stop the propagation of brittle cleavage cracks [11,33]. Obviously, the bainite grain size was greatly refined and the HAGBs fraction increased in the NZ of FSW-a joint, and thus the cleavage fracture may be inhibited with no straight large cracks observed on the surface morphology after impact test (Fig. 10c). Therefore, it could be considered that the refined prior austenite or bainite packets could effectively stop the propagation of brittle cleavage cracks and the propagation direction could be changed, as shown in Fig. 10d, which was also confirmed by Wang et al. [34]. Therefore, enhanced toughness without brittle cleavage fracture was achieved in the refined bainite structure of FSW-a joint.

From the investigation results, it is clear that FSW is indeed an effective method of refining the microstructure in the weld nugget. Moreover, compared to the fusion weld metal, enhanced strength

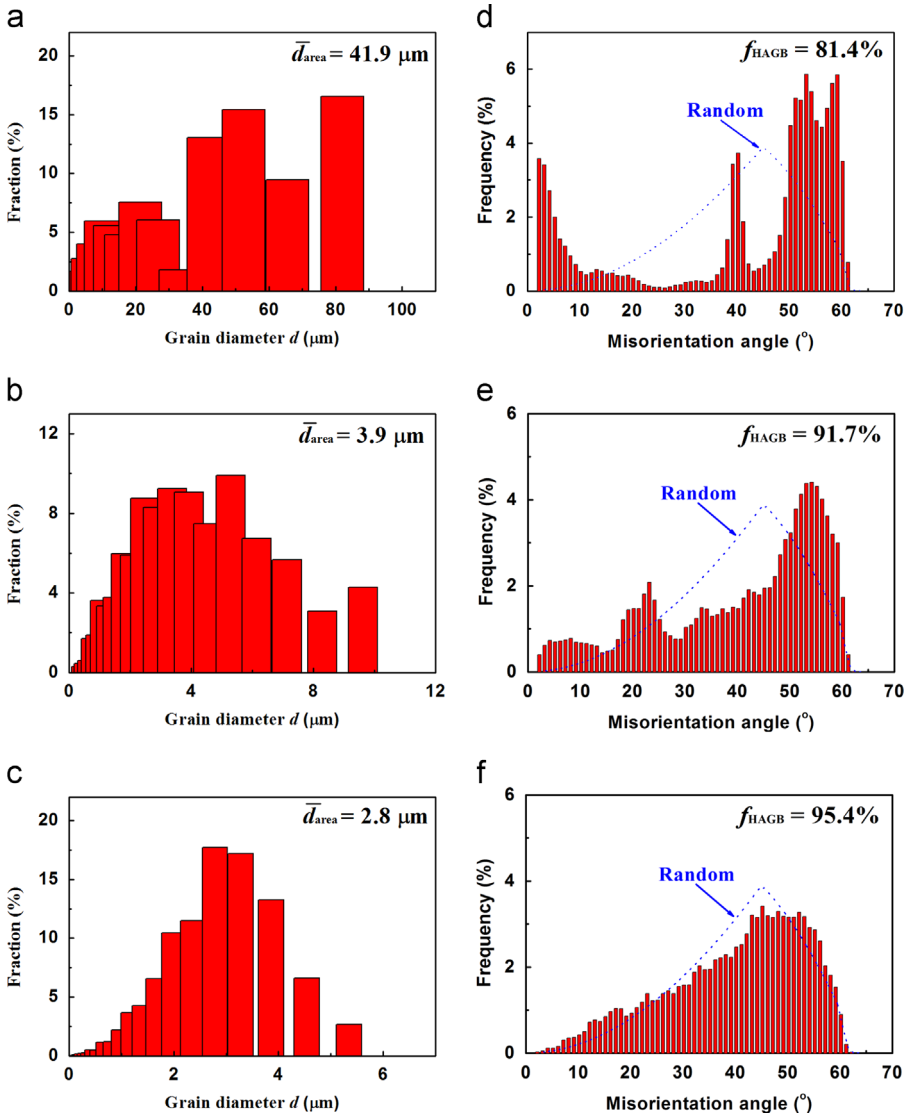

Fig. 6. Grain size distribution maps of (a) weld metal, (b) NZ in FSW-a joint, (c) NZ in FSW-b joint, and misorientation angle distribution maps of (d) weld metal, (e) NZ in FSW-a joint, and (f) NZ in FSW-b joint.

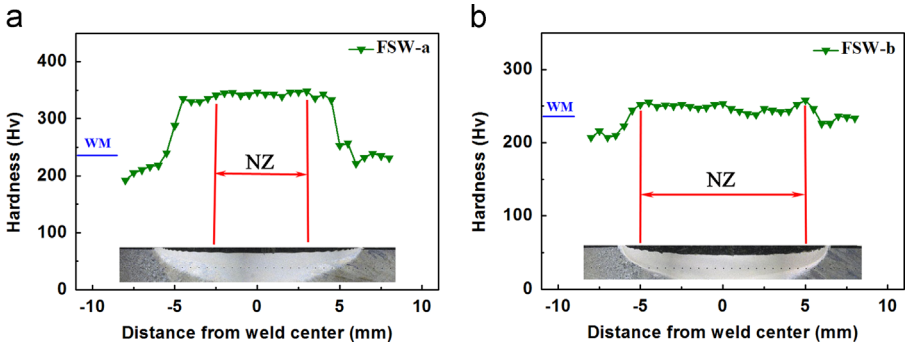

Fig. 7. Hardness distribution maps of (a) FSW-a joint and (b) FSW-b joint.

and toughness could be achieved in the refined microstructure. The abundant phase transformations exist in steels provide a good chance to design the best phase structure in the weld metal. FSW is able to produce various refined phase structures via adjusting the parameters, which may bring sound mechanical properties. Therefore, further studies to investigate the refining mechanism and the mechanical properties of the various refined phase structures in FSW steel joints are still demanding for future investigations.

5. Conclusions

In this study, the submerged arc weld metal was subjected to FSW at a higher rotation rate of 400 rpm (FSW-a) and a lower rotation rate of 125 rpm (FSW-b), respectively. The relationship of the microstructure and the mechanical properties for the weld metal and NZs were investigated. Main achievements of this study are summarized as follows.

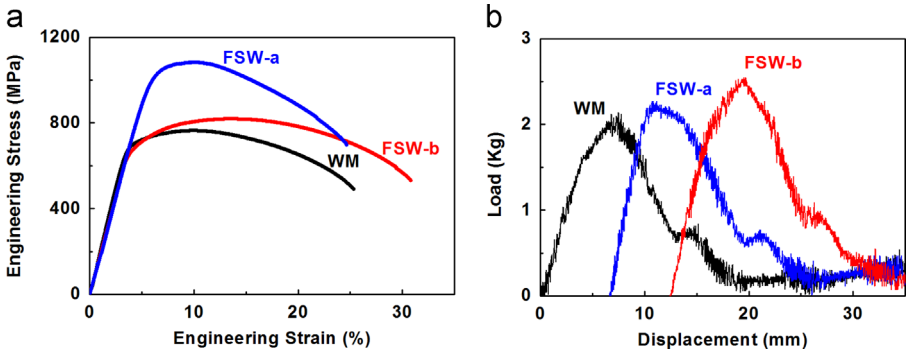

Fig. 8. (a) Tensile engineering stress–engineering strain curves, and (b) impact load–displacement curves of weld metal (WM) and NZs in both FSW joints (impact energies are determined by integrating area under each curve).

Table 3
Mechanical properties of the weld metal (WM) and NZs in both FSW joints.

Sample	YS (MPa)	UTS (MPa)	UE (%)	EL (%)	Impact energy (N mm)
WM	659 ± 1	761 ± 4	6.3 ± 0.1	23.0 ± 0.4	190 ± 2
FSW-a	955 ± 15	1056 ± 24	4.6 ± 0.3	19.5 ± 1.2	206 ± 7
FSW-b	634 ± 1	850 ± 30	11.6 ± 0.6	28.7 ± 0.8	251 ± 4

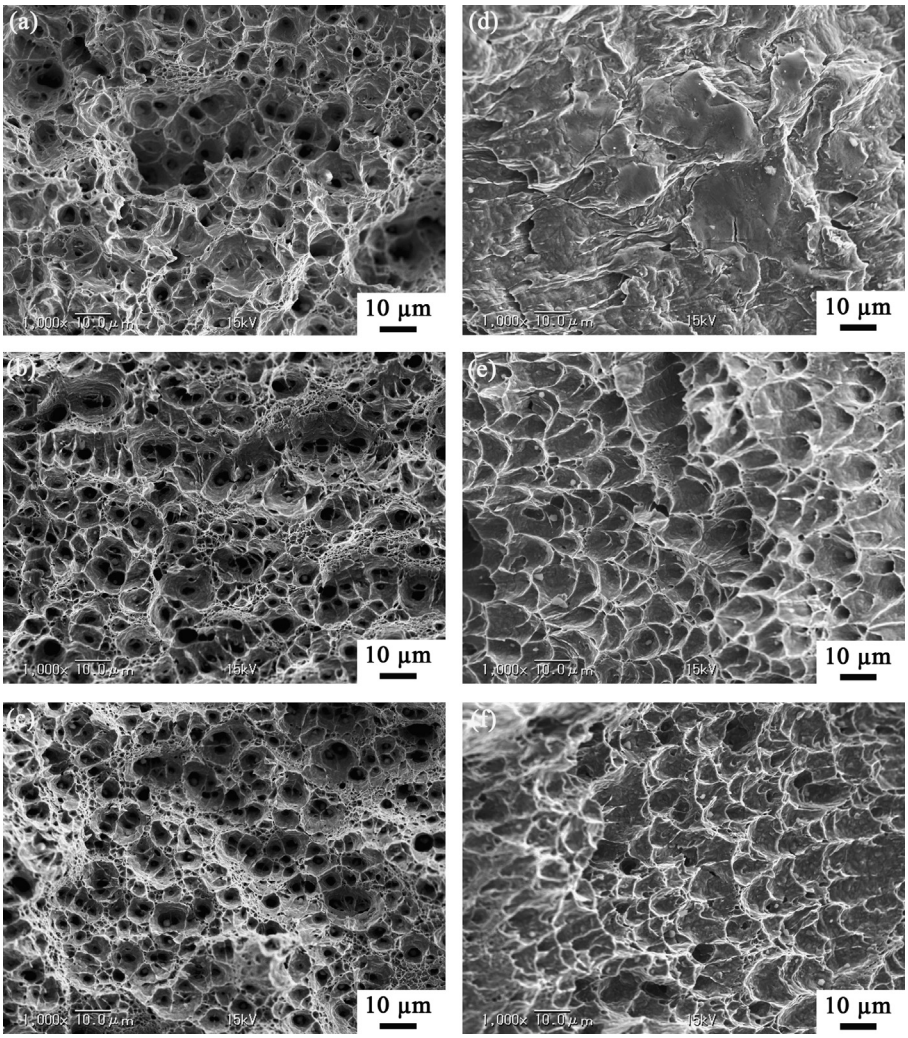

Fig. 9. SEM microstructure of fractured surfaces after tensile tests: (a) weld metal, (b) NZ in FSW-a joint, (c) NZ in FSW-b joint, and after impact tests: (d) weld metal, (e) NZ in FSW-a joint, (f) NZ in FSW-b joint.

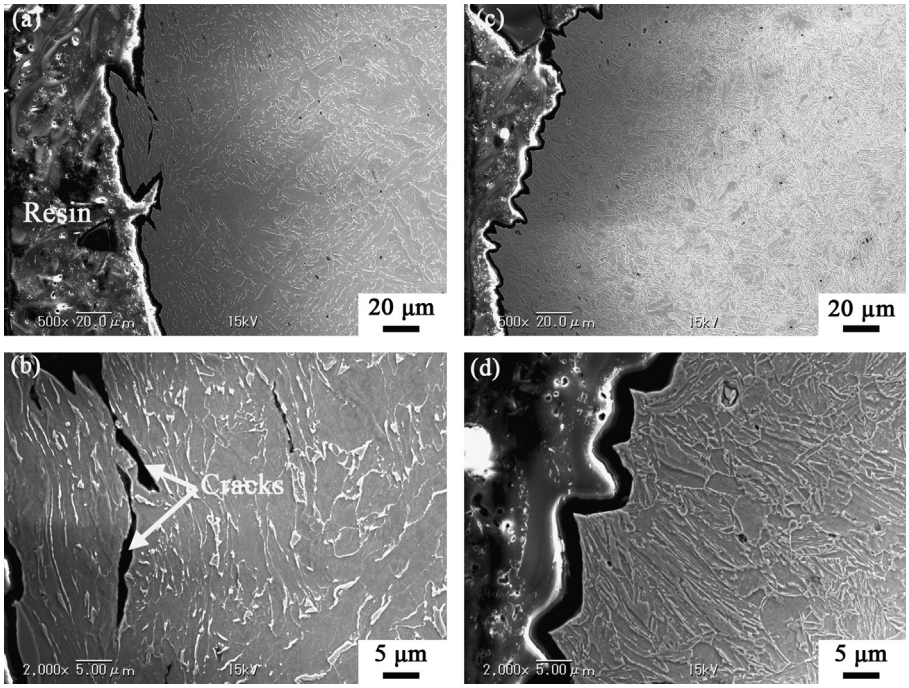

Fig. 10. SEM microstructure of surfaces after impact tests: (a) and (b) weld metal, (c) and (d) NZ in FSW-a joint.

1. The initial weld metal was characterized as coarse bainite phase structure, of which the lath boundaries were mainly LAGBs. Different peak temperatures of above A_{C3} and below A_{C1} were achieved in the NZs of FSW-a and FSW-b joints, resulting in refined bainite phase and ferrite phase, respectively.
2. Compared to the weld metal with a UTS of 761 MPa, the UTS increased to 1056 MPa in the fine bainite structure of the NZ of FSW-a joint, while the UE decreased slightly. Enhanced UTS of 850 MPa together with a high UE of 11.6% were achieved in the NZ of FSW-b joints, resulting from the greatly refined ferrite phase.
3. Large cracks easily propagated along the bainite lath boundaries in the coarse bainite grains of the weld metal, and the quasi-cleavage fracture morphology was observed on the impact fractured surface. However, the refined bainite structure in the NZ of FSW-a joint could effectively stop the propagation of large brittle cleavage cracks, resulting in an enhanced absorbed energy, and dimple fracture morphology was observed. Benefited from the fine ductile ferrite phase, dimple impact fracture with the highest absorbed energy were achieved in the NZ of FSW-b joint.

References

[1] C.Y. Chen, H.W. Yen, F.H. Kao, W.C. Li, C.Y. Huang, J.R. Yang, S.H. Wang, Mater. Sci. Eng. A 499 (2009) 162–166.
[2] B. Hwang, C.G. Lee, Mater. Sci. Eng. A 527 (2010) 4341–4346.
[3] X.J. Sun, Z.D. Li, Q.L. Yong, Z.G. Yang, H. Dong, Y.Q. Weng, Sci. China Technol. Sci. 55 (2012) 1797–1805.
[4] B.C. Kim, S. Lee, N.J. Kim, D.Y. Lee, Metall. Trans. A 22 (1991) 139–149.
[5] H.K.D.H. Bhadeshia, L.E. Svensson, J. Mater. Sci. 24 (1989) 3180–3188.
[6] R.A. Farrar, P.L. Harrison, J. Mater. Sci. 22 (1987) 3812–3820.
[7] D. Zhang, H. Terasaki, Y. Komizo, Acta Mater. 58 (2010) 1369–1378.
[8] F.R. Xiao, B. Liao, Y.Y. Shan, G.Y. Qiao, Y. Zhong, C.L. Zhang, K. Yang, Mater. Sci. Eng. A 431 (2006) 41–52.
[9] A.R. Mills, G. Thewlis, J.A. Whiteman, Mater. Sci. Technol. 3 (1987) 1051–1061.
[10] A. Takada, H. Terasaki, Y. Komizo, Sci. Technol. Weld. Join. 18 (2013) 91–96.
[11] L.Y. Wei, T.W. Nelson, Mater. Sci. Eng. A 556 (2012) 51–59.
[12] H.K.D.H. Bhadeshia, J.W. Christian, Metall. Trans. A 21 (1990) 206–215.
[13] R.S. Mishra, Z.Y. Ma, Mater. Sci. Eng. R 50 (2005) 1–78.
[14] R. Nandan, T. DebRoy, H.K.D.H. Bhadeshia, Prog. Mater. Sci. 53 (2008) 980–1023.
[15] M.A. Sutton, B. Yang, A.P. Reynolds, R. Taylor, Mater. Sci. Eng. A 323 (2002) 160–166.
[16] P. Xue, B.L. Xiao, Q. Zhang, Z.Y. Ma, Scr. Mater. 64 (2011) 1051–1054.
[17] G.M. Xie, Z.Y. Ma, L. Geng, R.S. Chen, Mater. Sci. Eng. A 471 (2007) 63–68.
[18] Y. Zhang, Y.S. Sato, H. Kokawa, S.H.C. Park, S. Hirano, Mater. Sci. Eng. A 485 (2007) 448–455.
[19] H. Bhadeshia, T. DebRoy, Sci. Technol. Weld. Join. 14 (2009) 193–196.
[20] P. Xue, B.L. Xiao, W.G. Wang, Q. Zhang, D. Wang, Q.Z. Wang, Z.Y. Ma, Mater. Sci. Eng. A 575 (2013) 30–34.
[21] Y.S. Sato, P. Arkom, H. Kokawa, T.W. Nelson, R.J. Steel, Mater. Sci. Eng. A 477 (2007) 250–258.
[22] M. Matsushita, Y. Kitani, R. Ikeda, S. Endo, H. Fujii, ISIJ Int. 52 (2012) 1335–1341.
[23] T.F.A. Santos, T.F.C. Hermenegildo, C.R.M. Afonso, R.R. Marinho, M.T.P. Paes, A. J. Ramirez, Eng. Fract. Mech. 77 (2010) 2937–2945.
[24] M. Abbasi, T.W. Nelson, C.D. Sorensen, Metall. Mater. Trans. A 43 (2012) 4940–4946.
[25] Y.D. Chung, H. Fujii, R. Ueji, N. Tsuji, Scr. Mater. 63 (2010) 223–226.
[26] H. Fujii, Y.D. Chung, Y.F. Sun, Sci. Technol. Weld. Join. 18 (2013) 500–506.
[27] A. Kimura, A. Koya, T. Morimura, T. Misawa, Mater. Sci. Eng. A 176 (1994) 425–430.
[28] A.P. Reynolds, Mater. Sci. Forum 539–543 (2007) 207–214.
[29] P. Xue, G.M. Xie, B.L. Xiao, Z.Y. Ma, L. Geng, Metall. Mater. Trans. A 41 (2010) 2010–2021.
[30] Y.S. Sato, M. Urata, H. Kokawa, Metall. Mater. Trans. A 33 (2002) 625–635.
[31] M. Matsushita, Y. Kitani, R. Ikeda, M. Ono, H. Fujii, Y.D. Chung, Sci. Technol. Weld. Join. 16 (2011) 181–187.
[32] S.J. Barnes, A.R. Bhatti, A. Steuwer, R. Johnson, J. Altenkirch, P.J. Withers, Metall. Mater. Trans. A 43 (2012) 2342–2355.
[33] V. Pancholi, M. Krishnan, I.S. Samajdar, V. Yadav, N.B. Ballal, Acta Mater. 56 (2008) 2037–2050.
[34] C.F. Wang, M.Q. Wang, J. Shi, W.J. Hui, H. Dong, Scr. Mater. 58 (2008) 492–495.